ORIGINAL PAPER

Synthesis and characterization of nitrogen-doped TiO$_2$ nanoparticles prepared by sol–gel method

**V. Caratto · L. Setti · S. Campodonico ·
M. M. Carnasciali · R. Botter · M. Ferretti**

Abstract The N-doped TiO$_2$ has been synthesized by sol–gel method, using titanium isopropoxide, isopropanol and an aqueous solution of ammonia with ratio 2:1:10. The concentrations used for the NH$_3$ aqueous solution were 3, 7, 10 and 15 %. The samples have been analysed by X-ray diffraction, electron microscopy (SEM and TEM) thermogravimetric analysis (TGA), differential scanning calorimetry (DSC), micro-Raman spectroscopy and diffuse reflectivity. TEM, SEM, DSC and TGA showed that the morphology is influenced by the presence of N^{3-} ions but not by the concentration of the solution. Instead reflectance gave us a relation between values of the energy gap and the concentration of N^{3-} ions: the gap between valence and conduction band lowers as the concentration of NH$_3$ in the starting solution increases. From these results we can say that the properties of the material have been tuned by doping with nitrogen ions because the particles absorb more light in the visible range, and this is important for photovoltaic and photocatalytic applications.

Keywords Photocatalysis · N-doped TiO$_2$ · Sol–gel method · Nanoparticles · Visible-light sensitization · Photovoltaic

V. Caratto (✉) · L. Setti · S. Campodonico ·
M. M. Carnasciali · M. Ferretti
Dipartimento di Chimica e Chimica Industriale, Università di Genova, Via Dodecaneso 31, 16146 Genoa, Italy
e-mail: caratto@chimica.unige.it

V. Caratto · L. Setti · M. Ferretti
CNR-SPIN, Corso Perrone 24, 16156 Genoa, Italy

R. Botter
Dipartimento di Ingegneria Chimica e di Processo, Università di Genova, Via dell'Opera Pia 15, 16134 Genoa, Italy

1 Introduction

Titanium dioxide (TiO$_2$), a large-band gap semi-conductor, has been widely studied because of its unique optical and chemical properties. Applications in photocatalysis [1], e.g. for advanced photochemical applications [2] interfacing with organic molecules (DNA included [3]), solar energy production [4, 5], and water treatment [6] are the main reasons to investigate the surface properties of such a material. At room temperature and pressure, TiO$_2$ exists in three natural polymorphs, i.e. anatase, brookite, rutile. Rutile is thermodynamically more stable than anatase [7–9]. When TiO$_2$ is irradiated by light with wavelength $\lambda < 387$ nm, electrons are promoted across the band gap (3.2 or 3.0 eV in the anatase or rutile crystalline phase, respectively) into the conduction band, leaving holes in the valence band [10–12]. These holes have high oxidation power, then react with adsorbed hydroxide ions to produce hydroxyl radicals, the main oxidizing species responsible for the photooxidation of organic compounds [11]. However, the application of pure TiO$_2$ is limited, because it requires UV activation. With pure TiO$_2$, only less than 5 % of the solar radiation reaching the surface of the earth can be used; consequently, considerable effort has been directed toward expanding the optical response of TiO$_2$ from the UV to the visible light region. One way to introduce allowed energy states in the band gap of TiO$_2$ by doping with transition metal ions such V, W, or Fe [12–17], but these doped materials are unstable. Another approach is to modify TiO$_2$ with nonmetal atoms, such as S, C, or N [18–23]. Burda et al. [24] performed nitrogen doping at room temperature by employing the direct amination of TiO$_2$ nanoparticles whereas Sathish et al. [25] synthesized nitrogen doped TiO$_2$ with spherical shape and homogeneous size through a chemical method using TiCl$_3$ as

precursor. In both cases light absorption onset shifts to the visible region.

Ohno et al. [26] found that the absorption edge of TiO_2 was largely shifted from 400 to 700 nm by doping carbonate species into the TiO_2 lattice. Wang et al. [27] prepared a C-doped TiO_2 catalyst using a nonhydrolytic sol–gel method and found that substitutional and interstitial carbon atoms coexisted in the lattice of TiO_2; the most important part of research is the ability to create reproducible samples with the same characteristics and properties. The control of the reaction could be done by selecting the proper reactants [28] and varying the relative percentage of the dopant precursor [29–32]. In the present work we synthesized nitrogen-doped TiO_2 nanoparticles using the sol–gel method.

2 Experimental procedure

Titania has been doped with different percentage of nitrogen starting from a solution of H_2O and NH_3 with four different volume concentration (3, 7, 10, 15 %). In the text the samples are identified using the notation $TiO_2N_{x\%}$ where x is the percentage of NH_3 in the starting solution. Synthesis of doped titania was carried out using sol–gel technique: an aqueous solution of NH_3 was introduced under stirring with titanium isopropoxide and 2-propanol. The first step is to mix titanium isopropoxide, isopropanol and water under vigorous stirring for 4 h in order to create a white mellow gel; then the mixture undergoes a thermal treatment at 100 °C for 12 h in order to eliminate the residual water and organic compounds still trapped inside and densify the amorphous aerogel [29]. At last the material undergoes calcination, performed in mitten, which is necessary to obtain crystalline nano-scaled powder. The control of the temperature allows to obtain different crystal structures: in the undoped samples a treatment at 350 °C for 1 h is sufficient to have the complete conversion in anatase, and a treatment at 700 °C for 1 h totally converts anatase into rutile. In order to have a reference, an undoped sample has been also synthesised, using deionized water instead of the aqueous ammonia solution. All the samples, including this last one, have undergone the same subsequent thermal treatments.

The samples have been analysed by X-ray diffraction (XRD), electron microscopy (SEM and TEM) thermogravimetric analysis (TGA), differential scanning calorimetry (DSC), micro-Raman spectroscopy and diffuse reflectivity.

Phase identification was performed by X-ray powder diffraction analysis using a Philips PW1830 diffractometer (Bragg–Brentano geometry; Cu Kα; Ni filtered; range 20–80° 2θ; step 0.025° 2θ; sampling time 10 s); the

crystalline structures were refined according to the Rietveld method using the Fullprof program.

Scanning electron microscopy (SEM) was performed using a Cambridge S360 microscope on powders coated with gold in low vacuum.

Transmission electron microscopy (TEM) was performed using a Joel JEM 2010 (200 kV, Lanthanum Boride crystal) microscope, and the energy dispersive spectroscopy (EDS) was performed using an Oxford link Pentafet (Si–Ge) instrument.

Micro-Raman spectroscopy was performed using a RENISHAW 2000 SYSTEM microspectrometer with a laser He–Ne $\lambda = 632.8$ nm.

Differential scanning calorimetry (DSC) and thermogravimetry (TG) were performed using a NETZSCH STA 409 thermobalance with a sensitivity of 0.1 mg, using 6 mm platinum crucible with lid in static air. Crucibles were filled with different amounts of powders depending on powder tap density and weighted with a precision balance (±0.1 mg). As a reference, a crucible filled with the same weight of calcined kaolin was used. Samples were heated at 1,200 °C with a heating rate of 10 °C/min, and TG and DSC baselines were acquired for each run repeating the same heating programme.

Diffuse reflectance spectroscopy was performed using a JASCO V-570 UV–VIS-NIR spectrophotometer.

3 Results and discussions

3.1 XRD analysis

Samples doped with every NH_3 concentration and thermally treated at 350 °C for 1 h show anatase structure. It is not present any other phase. The XRD pattern (Fig. 1) shows a small shift of the peaks in relation to the
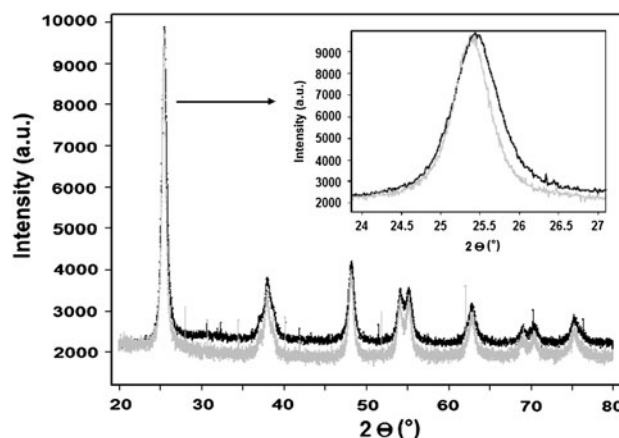
Fig. 1 XRD patterns of TiO_2 anatase (*black*) and $TiO_2N_{10\%}$ anatase (*grey*). The *inset* shows the shift of the peaks in the doped sample

concentration of the NH_3 of the starting solution which could indicate an enlargement of the cell. In fact, increasing the N^{3-} ion content in the solid solution, the steric hindrance increases. From structural refinement the cell parameter a (see Table 1) remains almost constant while c and the volume seem to increase until saturation. This trend could be due to a lattice strain induced by the change in particle morphology (as discussed later) or to the formation of an interstitial solid solution with a limited amount of doping.

Undoped samples undergo a phase transition to rutile structure after thermal treatment in the temperature range 700–900 °C while the sample doped with 10 % NH_3 treated at 700 and 900 °C for 3 h, did not completely convert in the rutile structure (Fig. 2). All thermal treatments gave the coexistence of anatase, rutile and a third phase recognised as titanium nitride (osbornite-type) by means of a comparative analysis using Pearson's Crystal Data. These results suggest that the anatase structure is stabilised by N doping and high temperature treatments lead to a reduction of N solubility.

3.2 SEM analysis

The analyses of samples show that the presence of nitrogen changes the morphology (Fig. 3). Undoped anatase grains

Table 1 Refined cell parameters for anatase structure of undoped TiO_2 and nitrogen-doped samples

%NH_3	a	c	V
0	3.7867 (6)	9.482 (2)	135.96 (4)
3	3.7857 (4)	9.4695 (9)	135.71 (3)
7	3.7867 (2)	9.5086 (5)	136.34 (1)
10	3.7854 (2)	9.5012 (4)	136.15 (1)
15	3.7872 (3)	9.4953 (8)	136.19 (2)
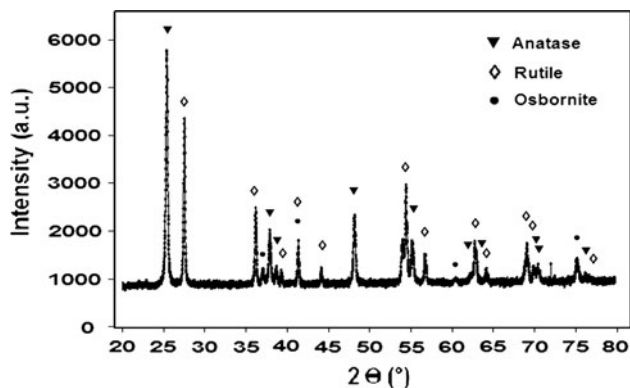
Fig. 2 XRD pattern of $TiO_2N_{10\%}$ after high temperature treatment at 900 °C. The rutile crystal structure coexists with anatase and osbornite
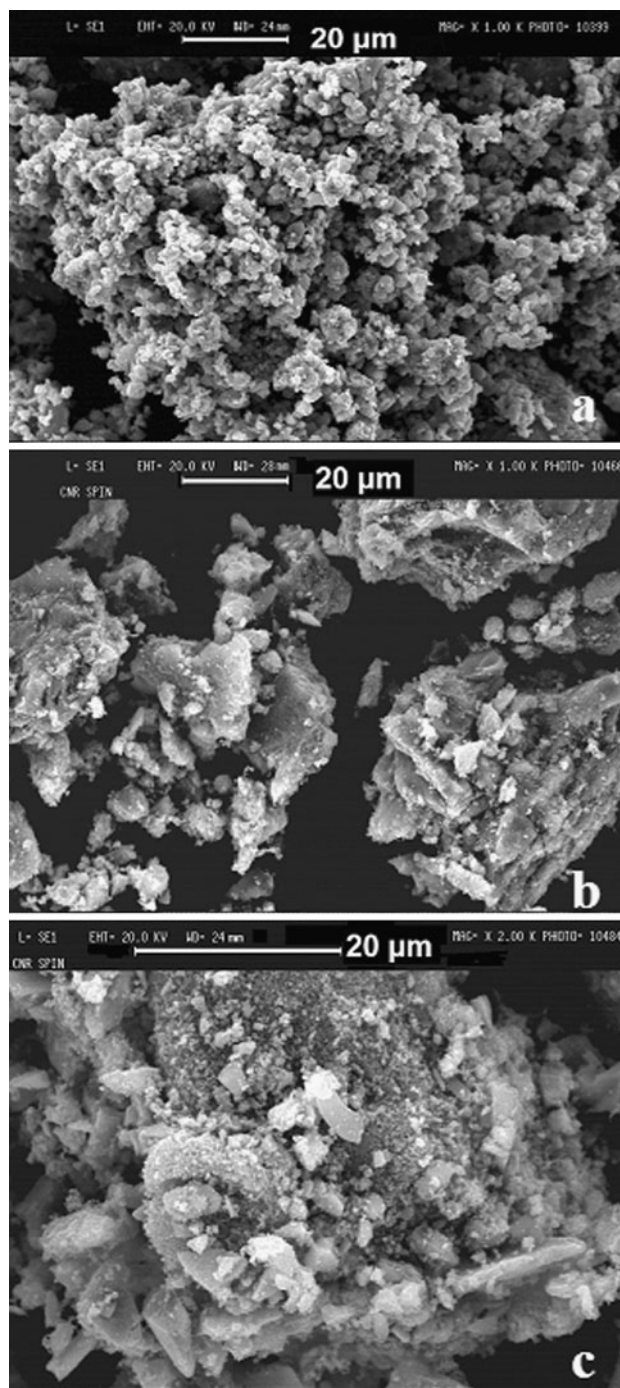
Fig. 3 The SEM image (reference length: 20 μm, magnification: ×1,000, EHT: 20 kV) shows a comparison among aggregates of undoped anatase (**a**) and TiO_2 $N_{15\%}$ anatase lamellae (**b**); also a $TiO_2N_{3\%}$ (**c**) group of aggregates is shown using an higher magnification (×2,000)

have rounded shape and form sponge-like aggregates, while nitrogen doped anatase forms lamellar isolated aggregates. The variation of the amount of N^{3-} ions inside the crystal structure does not imply any further morphological change, even at higher magnification (Fig. 3c). The

reason is that the shape stability of TiO_2 nanoparticles is highly dependent on surface chemistry, and the synthesis conditions play a key role. According to theoretical models [33], in the case of hydrogenated, hydrogen-rich, and hydrated surfaces, the shape of anatase and rutile nanoparticles vary very little with surface chemistry (with only slight changes in the aspect ratio evident); however, in the case of hydrogen-poor and oxygenated surfaces, that is in presence of a base such as NH_3, nanocrystals of both polymorphs become elongated, and this could lead to the formation of lamellar aggregates.

3.3 TEM analysis

The analysis was performed on samples $TiO_2N_{3\%}$ and $TiO_2N_{15\%}$ (Fig. 4). In both samples the shape is more angular and a little more elongated respect to the undoped TiO_2. There is no evidence that the increase of the NH_3 concentration modifies the crystallisation process, the shape and dimensions of nanoparticles. This evidence is also confirmed by the analysis of grain size of samples (Fig. 6), and may signify that there is an effect of saturation of the adsorbates on the surface sites as previously pointed out. The grain size of pure anatase is 19 ± 2 nm, while for $TiO_2N_{3\%}$ and for $TiO_2N_{15\%}$ is 17 ± 2 nm, so we can assess that the presence of nitrogen does not influence the average dimension of the nanoparticles without any significant

difference in the whole range of concentration, while the aspect ratio is slightly tuned. This evidence is complementary and confirms the results of the SEM analysis.

Comparing TEM and SEM analysis, it is possible to assess that N^{3-} ions influence the shape of the particles and aggregates, shifting from a rounded sponge-like shape to a lamellar angular one. The particles have essentially the same size; moreover the increase of the concentration of nitrogen in the starting solution does not produce any further morphological change.

3.4 Micro Raman analysis

Samples were prepared as thin film on glass substrates, and analysed immediately.

The analysis on TiO_2N_x specimens obtained from ammonia in aqueous solution at different concentrations (3, 7, 10, 15 %) was repeated several times in different points to verify the homogeneity of the samples.

Vibrational modes of TiO_2 were identified according to literature [34, 35]. In Fig. 5 are represented the spectra superposition of pure titania, $TiO_2N_{3\%}$ and $TiO_2N_{15\%}$. The analyses did not show new peaks due to the introduction of nitrogen: this consideration leads to assess that N^{3-} ions probably did not occupy substitutional positions of the anatase crystal structure, but interstitial ones, which only partially influence vibrational modes of TiO_2. Magnification
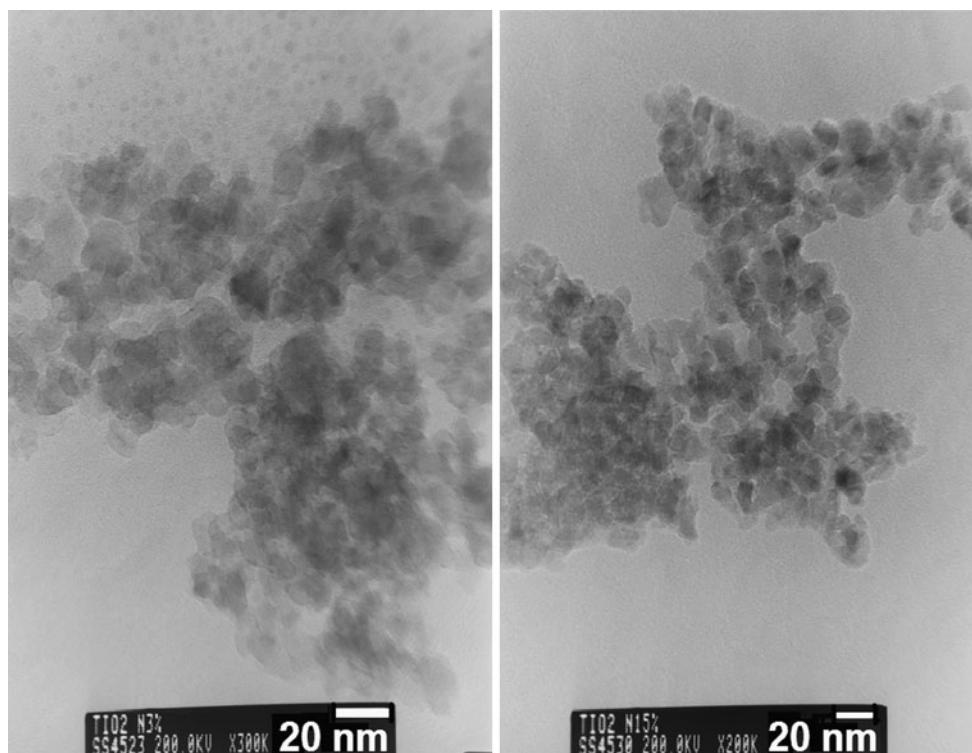
Fig. 4 TEM image of $TiO_2N_{3\%}$ (×300, *left*) and $TiO_2N_{15\%}$ (×200, *right*) powders
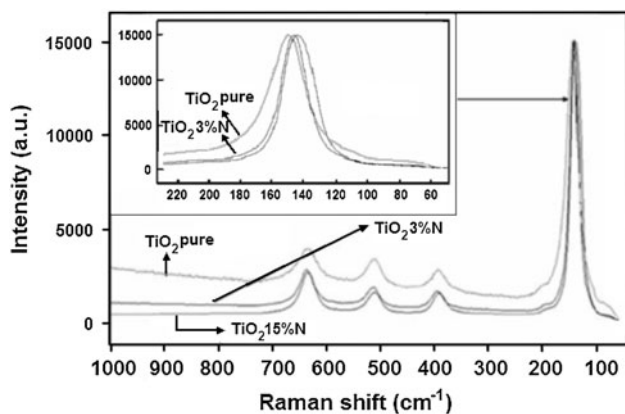
Fig. 5 Micro-Raman spectra of pure anatase (*top line*), $TiO_2N_{3\%}$ (*central line*), $TiO_2N_{15\%}$ (*bottom line*). Power: 25 %, Acc. 10, Time: 1 s, Obj.: ×50, static scan: 540 nm

of the peak set to 146 cm^{-1}, due to bending vibration of O–Ti–O bonds, shows a peak shift of 4–6 cm^{-1}, which is higher than the spectral resolution of the instrument (3 cm^{-1}). This could confirm the presence of N^{3-} ions in interstitial sites, creating an hindrance and modifying the normal vibrational modes of TiO_2. In the figure, the line labelled as "pure" identifies the normal position of the peak at 146 cm^{-1}, which shifts towards 142 cm^{-1} for $TiO_2N_{3\%}$, while for $TiO_2N_{15\%}$ reaches 140 cm^{-1}. Modes of $TiO_2N_{7\%}$ and $TiO_2N_{10\%}$ fall between peaks of $TiO_2N_{3\%}$ and $TiO_2N_{15\%}$ and the shift of the other peaks remains below the spectral resolution of the micro-spectrophotometer. From this consideration, we can hypothesise that the N^{3-} ions enter in interstitial position in relation to the concentration of nitrogen in the starting solution, until saturation. Probably, the saturation level is reachable starting from an aqueous solution of ammonia 3 %, in fact the shift at higher concentration of the solution is comparable with the instrument sensitivity.

3.5 TGA-DSC analysis

The undoped and $TiO_2N_{3\%}$ samples were compared both after the drying process and after the heat treatment at 350 °C, and every measure has been repeated two times in order to ensure the goodness of the acquired data and to eliminate any possible artifact. However, all the doubled measures were in agree.

In Fig. 6 it is shown the weight loss curve for undoped anatase and $TiO_2N_{3\%}$ previously dried at 100 °C, with the corresponding DSC spectra overplotted and referred to a secondary axe in order to better compare the informations. The undoped sample shows a larger overall weight loss, which takes places in different regions: the first step, which is at lower temperatures, can be assigned to the loss of the remaining water; a second step, which begins around
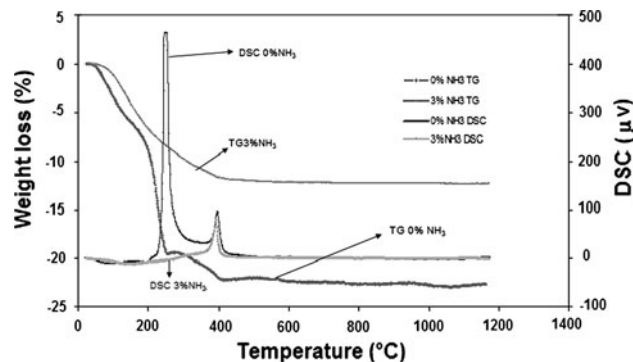
Fig. 6 Thermogravimetric scan (T: 0–1,170 °C, rate: 10 °C/min) of pure anatase and $TiO_2N_{3\%}$ dried samples. The DSC signal is superposed in order to facilitate the interpretation

240 °C, is due to the oxidation of isopropanol adsorbed on the surface, and is correlated to a strong exothermic peak observable in the DSC plot. Both samples show an exothermic peak at 400 °C in correspondence of a phase transition of TiO_2, which crystallises in the anatase structure starting from the amorphous form.

In Fig. 7 it is shown the weight loss curve for undoped anatase and $TiO_2N_{3\%}$ after the heat treatment at 350 °C, with the corresponding DSC spectra overplotted. It is important to notice that approximately the 4 % of the initial mass corresponds to water readsorbed on the surface of the powders while cooling from 350 °C to room temperature (as confirmed from the DSC endothermic peak at 100 °C). Chemically adsorbed water has a stronger bond with the surface, and is released up to 600 °C in a broad range of temperatures. The undoped sample shows a weight loss which is 15 % larger than the $TiO_2N_{3\%}$ one, and also an exothermic peak around 700 °C, due to the phase transition from anatase to rutile. This transformation happens approximately 100 °C above the bulk transition temperature for pure TiO_2: thus, the contribution of the surface energy, which should not be neglected when
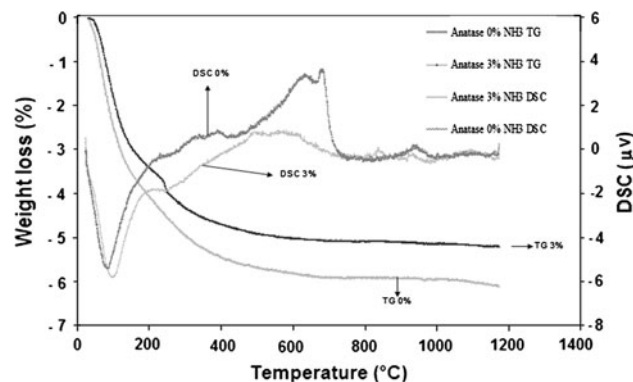
Fig. 7 Thermogravimetric scan (T: 0–1,170 °C, rate: 10 °C/min) of pure anatase and $TiO_2N_{3\%}$ samples after heat treatment at 350 °C. The DSC signal is superposed in order to facilitate the interpretation

treating nanopowders, stabilises the anatase phase. The nitrogen doping causes a further stabilisation of anatase: in fact, doped samples do not show any recrystallisation peak, and this is in agreement with XRD analyses.

The experimental results confirm that doped samples absorb less water because of a denser microstructure and lower surface area, as observed with SEM, and that nitrogen doping leads to the stabilisation of the anatase structure. Moreover it was found that undoped powders were sintered after thermogravimetric analyses, while doped samples remained loose powders. This evidence is critical from the practical point of view because, even though doped samples show a lower surface area, these ones are more stable and could be used in more severe environments, which are very common in chemical plants.

3.6 Diffuse reflectance analysis

Since the colour of powders varies visibly with the concentration of N^{3-} inside the crystal structure, we decided to measure the diffuse reflectance, which is a common analysis for the study of powders. A beam illuminates the sample and penetrates for few atomic layers, where is reflected or scattered. A change in the band position and in the shape of the peak gives a clear information about the elements and the bonds of the substance. The radiation is collected with special integrating spheres, and the output is a spectrum in terms of absorbance or reflectance. Samples were prepared in tablets, pressing 400 mg of powders at 4 atm, and every scan has been performed on a new tablet, in order to have reliable results. The superposition of the spectra shows the different behaviour of the doped anatase respect to the pure one. In the visible region there is an edge of absorption which shifts to lower wave-numbers for samples synthesized with higher concentrations of NH_3. Using the wavelength corresponding to the edge of the experimental spectrum, we derived the E_{gap} of each sample using the relation: $\Delta e_{gap} = c/\lambda$. The results listed in Table 2 show that the increase of the concentration of NH_3 in the solution corresponds to the shift of the absorption edge towards the visible region, due to the decrease of the energy gap. The decrease of the energy gap is consistent

Table 2 Values of wavelength and the energy gap calculated for undoped anatase and nitrogen-doped samples

%NH$_3$	Wavelength (nm)	Energy gap (eV)
0	384	3.642
3	398	3.123
7	402	3.092
10	407	3.054
15	413	3.009

with literature [36], and is a very important result, because this allows the use of natural light for photocatalytic reactions and photovoltaic applications.

4 Conclusions

The systematic study of nitrogen-doped TiO_2 plays a key role for enhancing the yield of the material, especially the photocatalytic activity. The optimisation of the material properties is in fact essential for any electronic device, filtration apparatus or sterilization system produced starting from powders.

The synthesis with the sol–gel method leads to the formation nanoparticles with sharp grain size distribution, and in sufficient amount to perform different types of analysis. Anatase was always synthesised without any problem, while the synthesis of rutile often presented phase separation, due to the difficulty to insert interstitial ions of dopant in the structure. In fact in the case of N^{3-} ions we obtained a mixture of rutile and titanium nitride.

Using different analysis techniques (XRD, SEM, TEM, Micro-Raman, Reflectometry) it was possible to understand the behaviour of the nitrogen inside the lattice. Doped samples have only anatase structure, and the XRD analysis revealed a shift of peaks due to the variation of cell parameters. It is not possible to say exactly if N^{3-} ions enter in substitutional or interstitial position using XRD only: for this reason we performed micro-Raman analysis, from whose results we hypothesised that nitrogen occupies interstitial positions. In order to have the definitive validation, we programmed neutron diffraction experiments at the Institut Laue-Langevin in Grenoble (France).

TEM, SEM, DSC and TG showed that the morphology is influenced by the presence of N^{3-} ions but not by the concentration. Reflectance gave us a relation between values of the energy gap and the concentration of N^{3-} ions. The gap between valence and conduction band lowers as the concentration of NH_3 in the starting solution increases.

From these results we can say that the properties of the material have been improved by doping with nitrogen ions, and the functionality of the devices produced using TiO_2 nanopowders coming from sol–gel reactions could be easily enhanced. In fact, the doping method is simple and can be applied on a large scale, the obtained material does not need to work under UV irradiation to be significantly efficient in photocatalysis, and the efficiency in photovoltaic applications can substantially increase, due to possibility to absorb a larger fraction of solar light. Moreover, even though doped samples show a lower surface area, these ones are more stable and could be used in more severe environments, which are very common in chemical plants.

References

1. Keshmiri M, Mohseni M, Troczynski T (2004) Appl Catal B 53(4):209–219
2. Yu J, Wang B (2010) Appl Catal B 94(3–4):295–302
3. Paunesku T, Ke T, Dharmakumar R, Mascheri N, Wu A, Lai B, Vogt S, Maser J, Thurn K, Szolc-Kowalska B, Larson A, Bergan RC, Omary R, Li D, Lu Z, Woloschak GE (2008) Nanomed—Nanotechnol Biol Med 4(3):201–207
4. Burke A, Ito S, Snaith H, Bach U, Kwiatkowski J, Grätzel M (2008) Nano Lett 8(4):977–981
5. Dohrmann JK, Schaaf NS (1992) J Phys Chem 96(11):4558–4563
6. Caballero L, Whitehead KA, Allen NS, Verran J (2009) J Photochem Photobiol A Chem 202(2–3):92–98
7. Muscat J, Swamy V, Harrison NM (2002) Phys Rev B 65:224112–224127
8. Gribb AA, Banfield JF (1997) Am Miner 82:717–728
9. Caratto V, Ferretti M, Setti L (2012) Appl Surf Sci 258(7):2393–2396
10. Yu J, Zhao X, Zhao Q (2000) Thin Solid Films 379(1–2):7–14
11. Zhang H, Banfield JF (1998) J Mater Chem 8(9):2073–2076
12. Chen GS, Guo SY, Zhang F (2011) Adv Mater Res 183–185:591–594
13. Chen X, Mao SS (2007) Chem Rev 107(7):2891–2959
14. Linsebigler AL, Lu G, Yates JT (1995) Chem Rev 95(3):35–758
15. Fox MA, Dulay MT (1993) Chem Rev 93(1):341–357
16. Klosek S, Raftery D (2001) J Phys Chem B 105(14):2815–2819
17. Surolia PK, Tayade RJ, Jasra RV (2007) Ind Eng Chem Res 46(19):6196–6203
18. Mohamed MM, Al-Esaimi MM (2006) J Mol Catal A 255 (1–2):53–61
19. Karakitsou KE, Verykios XE (1993) J Phys Chem 97(6):1184–1189
20. Yang S, Gao L (2004) J Am Ceram Soc 87(9):1803–1805
21. Cong Y, Zhang J, Chen F, Anpo M (2007) J Phys Chem C 111(19):6976–6982
22. Anpo M, Dohshi S, Kitano M, Hu Y, Takeuchi M, Matsuoka M (2005) Rev Mater Res 35:1–27
23. Ohno T, Mitsui T, Matsumura M (2003) Chem Lett 32(4):364–365
24. Burda C, Lou Y, Chen X, Samia ACS, Stout J, Gole JL (2003) Nano Lett 3(8):1049–1051
25. Sathish M, Viswanathan B, Viswanath RP, Gopinath CS (2005) Chem Mater 17(25):6349–6353
26. Ohno T, Tsubota K, Nishijima K, Miyamoto Z (2004) Chem Lett 33(6):750–751
27. Wang S, Meng S, Zhang X, Wang H, Zhong W, Du Q (2007) Chem Phys Lett 444(4–6):292–296
28. Hench LL, West JK (1990) Chem Rev 90(1):33–72
29. De la Romero Cruz D, Torres Torres G, Arévalo JC, Gomez R, Aguilar-Elguezabal A (2010) J Sol Gel Sci Technol 56(3):219–226
30. Liu Y, Chen X, Li J, Burda C (2005) Chemosphere 61(1):11–18
31. Chen X, Liu L, Mao S (2011) Science 331(6018):746–750
32. Periyat P, Pillai SC, McCormack DE, Colreavy J, Hinder SJ (2008) J Phys Chem C 112(20):7644–7652
33. Barnard AS, Curtiss LA (2005) Nano Lett 5(7):1261–1266
34. Oshaaka T, Izumi F, Fujiki Y (1978) J Raman Spectrosc 7(6):321–324
35. Hong NH, Sakai J, Poirot N, Brize V (2006) Phys Rev B 73:132404
36. Asahi R, Morikawa T, Ohwaki T, Aoki K, Taga Y (2001) Science 293(5528):269–271